


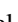




Structural spillage: An efficient method to identify noncrystalline topological materials

Daniel Muñoz-Segovia ^{1,2,*}, Paul Corbae ^{3,4,*}, Dániel Varjas ^{5,6}, Frances Hellman ^{3,4,7},
Sinéad M. Griffin ^{4,8,‡} and Adolfo G. Grushin ^{2,§}

¹Donostia International Physics Center, 20018 Donostia-San Sebastian, Spain

²University Grenoble Alpes, CNRS, Grenoble INP, Institut Néel, 38000 Grenoble, France

³Department of Materials Science, University of California, Berkeley, California 94720, USA

⁴Materials Sciences Division, Lawrence Berkeley National Laboratory, Berkeley, California, 94720, USA

⁵Department of Physics, Stockholm University, AlbaNova University Center, 106 91 Stockholm, Sweden

⁶Max Planck Institute for the Physics of Complex Systems, Nöthnitzer Strasse 38, 01187 Dresden, Germany

⁷Department of Physics, University of California, Berkeley, California 94720, USA

⁸Molecular Foundry Division, Lawrence Berkeley National Laboratory, Berkeley, California 94720, USA



(Received 23 February 2023; revised 25 May 2023; accepted 11 August 2023; published 12 October 2023; corrected 15 November 2023)

While topological materials are not restricted to crystals, there is no efficient method to diagnose topology in noncrystalline solids such as amorphous materials. Here we introduce the structural spillage, a new indicator that predicts the unknown topological phase of a noncrystalline solid, which is compatible with first-principles calculations. We illustrate its potential with tight-binding and first-principles calculations of amorphous bismuth, predicting a bilayer to be a new topologically nontrivial material. Our work opens up the efficient prediction of noncrystalline solids via first-principles and high-throughput searches.

DOI: [10.1103/PhysRevResearch.5.L042011](https://doi.org/10.1103/PhysRevResearch.5.L042011)

Introduction. Predicting which solids host nontrivial electronic topological phases is a central problem in condensed matter physics. For crystalline solids, first-principles methods take advantage of crystal symmetries to identify topological materials [1–5]. However, symmetry-based methods cannot be applied to diagnose nontrivial topology in materials that lack translational invariance such as amorphous, polycrystalline, and quasicrystalline materials. In fact, given the far greater ubiquity of noncrystalline materials in condensed matter, solving this challenge would open up several new material classes far more numerous than crystals, with both fundamental interest for novel phenomena unique to noncrystalline matter [6–39], and for their possible greater ease of integration into devices [40,41].

Prior work on topology in noncrystalline materials used convenient amorphous tight-binding models with average and local symmetries [11,14,20,21,42], however these do not include the full chemical and structural specificity found in real matter. Similarly, real-space invariants [8,43–55], including Wannier-based tight-binding formalism, require the system be treated on a case-by-case basis and can be computationally

costly. Single-point formulas constitute powerful tools for some classes [56,57], but general and efficient formulas are still lacking.

To overcome this methodological problem, we introduce the “structural spillage,” which is inherently compatible with first-principles approaches. Since the characterization of topology in general relies on the comparison with a known reference [58], we propose that in our case the appropriate comparison is between the wavefunctions of the noncrystalline target system and a crystalline reference state. A similar approach was proposed in Ref. [59] to identify topological band inversions in crystals by comparing the wavefunction overlap in insulating crystals with and without spin-orbit coupling (the *spin-orbit* spillage). The spillage is an example of a “strange correlator,” which diagnoses the topology of symmetry protected topological phases by comparing them to a trivial reference system [60,61].

As a strange correlator, the spillage relies on the non-Wannierizability of short-range entangled topologically nontrivial phases, i.e., the obstruction to find exponentially localized wavefunctions. This obstruction holds irrespective of the lattice structure [48,49,51,53], but the spillage is not currently applicable to noncrystalline systems. This is a significant drawback as it impedes the prediction of a potentially large number of novel topological materials, such as quasicrystals or amorphous solids.

In this work we introduce the *structural spillage* as a method to calculate the overlap between wavefunctions with different structural configurations. The central advantage of this method is the use of a crystal as the reference system, whose topological characterization can be efficiently calculated using standard symmetry-based methods [1–5], to determine whether noncrystalline systems retain the

*These authors contributed equally to this work.

†daniel.munozsegovia@dipc.org

‡sgriffin@lbl.gov

§adolfo.grushin@neel.cnrs.fr

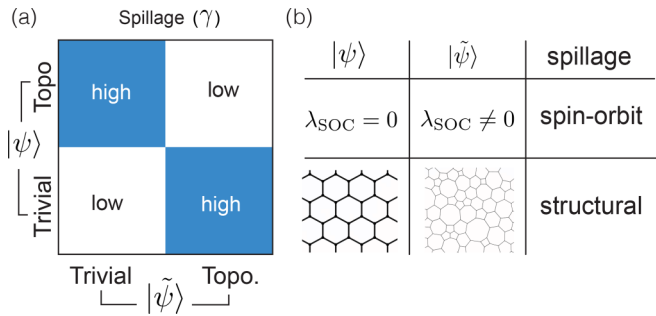


FIG. 1. (a) The spillage γ is high or low depending on whether a test wavefunction $|\psi\rangle$ is in the same or different topological state compared to a known reference wavefunction $|\tilde{\psi}\rangle$. (b) The spin-orbit spillage [59] compares wavefunctions with and without SOC. The structural spillage takes advantage of the knowledge of the topological state of a crystalline solid to find the topological state of an amorphous solid.

topological properties of their crystalline counterparts (Fig. 1). Our results indicate that the structural spillage can accurately identify amorphous bismuthene as topologically nontrivial [13,62], and predicts that amorphous bilayer bismuth is a novel topological material. By definition, the structural spillage is applicable to generic noncrystalline materials. It is suitable to establish a high-throughput catalog of potential noncrystalline topological materials, using currently available density functional theory (DFT) codes.

Structural spillage. The total spillage γ measures the mismatch between two projectors P and \tilde{P} into occupied states [59]

$$\gamma = \frac{1}{2} \text{Tr}[(P - \tilde{P})^2] = \text{Tr}[P(1 - \tilde{P})], \quad (1)$$

where the trace acts on the entire Hilbert space, and the last equality holds under the assumption that both systems have the same total number of occupied states $N_{\text{occ}} = \text{Tr}[P] = \text{Tr}[\tilde{P}]$. By definition, $\gamma \geq 0$ and can be viewed as the variance between two distributions with the same average. When $P = \tilde{P}$ the spillage vanishes. However, when the overlap between the two projectors is zero, it equals the total number of occupied states N_{occ} . Therefore, γ acts as an indicator of band inversions caused by the parameters that differ in P and \tilde{P} [59].

To predict topological band inversions in crystals, Liu and Vanderbilt [59] chose P and \tilde{P} to be projectors onto the subspace of occupied states of crystalline insulators with and without spin-orbit coupling (SOC), respectively. Lattice periodicity allows these to be written in Bloch momentum \mathbf{k} as $P(\mathbf{k}) = \sum_{n \in \text{occ}} |\psi_{n\mathbf{k}}\rangle \langle \psi_{n\mathbf{k}}|$, which defines a \mathbf{k} -resolved

spin-orbit Bloch spillage $\gamma_B(\mathbf{k}) = n_{\text{occ}} - \text{Tr}[P(\mathbf{k})\tilde{P}(\mathbf{k})]$, where $n_{\text{occ}} = N_{\text{occ}}/N_{\text{cells}}$ is the number of occupied bands. The total spillage is recovered by summing over all momenta in the Brillouin zone (BZ) $\gamma = \sum_{\mathbf{k}} \gamma_B(\mathbf{k})$. The spin-orbit Bloch spillage $\gamma_B(\mathbf{k})$ thus quantifies the band inversion caused by SOC at each \mathbf{k} ; it is large at points in the BZ where the band inversion is sizable. Reference [59] showed that at certain points in the BZ the spin-orbit Bloch spillage has to be larger than some given value if the SOC induces a topologically nontrivial phase from Wannier obstruction arguments. For instance, this lower bound equals two for a time-reversal symmetric topological insulator.

From the above properties, $\gamma_B(\mathbf{k})$ can be used to signal topological band inversions in crystals, and is straightforward to calculate using DFT [59]. Indeed, it has recently been applied to high-throughput searches for topological crystals [63,64]. We note, however, that a large spillage is a necessary but not sufficient condition for nontrivial topology: in certain cases, e.g., when many bands close to the Fermi level are slightly mixed by SOC, the spillage may be fooled by trivial insulators [59]. Consequently, more recent searches for topological crystals favor symmetry-based methods. In most practical cases, the spillage is expected to be an accurate indicator of topology in crystals [59].

In this work, we propose a spillage that compares a noncrystalline system with the crystalline counterpart closest in local structure. In doing so, we take advantage of the well-developed methods of symmetry indicators for the topological characterization of crystals [2]. To this end, we now reformulate our spillage in a plane-wave basis for incorporation into standard plane-wave DFT codes. Moreover, it is also well defined for both crystalline and noncrystalline systems. We write the total spillage γ in the plane wave basis $|\mathbf{p}\alpha\rangle$, where \mathbf{p} is the plane-wave momentum (not necessarily restricted to the first BZ) and α denotes spin. To calculate the spillage, we need the projector onto occupied states of the amorphous and reference systems $P = \sum_{N \in \text{occ}} |\psi_N\rangle \langle \psi_N|$, where $|\psi_N\rangle$ are the eigenstates. By projecting these onto plane waves, we then have access to the projector matrix elements $P_{\mathbf{p},\mathbf{p}'}^{\alpha\beta} = \langle \mathbf{p}\alpha | P | \mathbf{p}'\beta \rangle$, which are well-defined for crystalline and noncrystalline systems. Any plane-wave momentum \mathbf{p} can be uniquely decomposed as $\mathbf{p} = \mathbf{k} + \mathbf{G}$, the sum of a crystal momentum \mathbf{k} in the first BZ plus a reciprocal lattice vector \mathbf{G} , both of the reference crystal. Then, by substituting the plane-wave expansion into Eq. (1), we can define the quasi-Bloch spillage as

$$\gamma_{\text{qB}}(\mathbf{k}) = \frac{1}{2} \sum_{\mathbf{k}'} \sum_{\mathbf{G}\mathbf{G}'} \sum_{\alpha\beta} [P_{\mathbf{k}+\mathbf{G},\mathbf{k}'+\mathbf{G}'}^{\alpha\beta} P_{\mathbf{k}'+\mathbf{G}',\mathbf{k}+\mathbf{G}}^{\beta\alpha} - P_{\mathbf{k}+\mathbf{G},\mathbf{k}'+\mathbf{G}'}^{\alpha\beta} \tilde{P}_{\mathbf{k}'+\mathbf{G}',\mathbf{k}+\mathbf{G}}^{\beta\alpha}] + [P \leftrightarrow \tilde{P}] = \quad (2a)$$

$$= \frac{1}{2} \left\{ \left[\sum_{\mathbf{G}\alpha} P_{\mathbf{k}+\mathbf{G},\mathbf{k}+\mathbf{G}}^{\alpha\alpha} \right] + \tilde{n}_{\text{occ}}(\mathbf{k}) - \sum_{\mathbf{G}\alpha} \sum_{\mathbf{G}'\beta} [P_{\mathbf{k}+\mathbf{G},\mathbf{k}+\mathbf{G}'}^{\alpha\beta} \tilde{P}_{\mathbf{k}+\mathbf{G}',\mathbf{k}+\mathbf{G}}^{\beta\alpha} + \tilde{P}_{\mathbf{k}+\mathbf{G},\mathbf{k}+\mathbf{G}'}^{\alpha\beta} P_{\mathbf{k}+\mathbf{G}',\mathbf{k}+\mathbf{G}}^{\beta\alpha}] \right\} \quad (2b)$$

In Eq. (2b) we have used the fact that the reference projector \tilde{P} corresponds to a crystal, which allows us to set $\mathbf{k}' = \mathbf{k}$ in terms involving at least one \tilde{P} , since there is no scattering between different crystal momenta due to the discrete translational symmetry. Note that $\gamma_{\text{qB}}(\mathbf{k})$ fulfills the same sum rule as the Bloch spillage $\gamma = \sum_{\mathbf{k}} \gamma_{\text{qB}}(\mathbf{k})$. Therefore, applied to two insulating crystals, $\gamma_{\text{qB}}(\mathbf{k})$ recovers the Bloch spillage. Moreover, it can also be applied to semimetallic systems with the advantage of it being bounded by zero, in contrast to recent extensions to semimetallic materials [63,64].

Our key result is that the structural quasi-Bloch spillage, defined by Eq. (2), can be used as an efficient topological indicator in noncrystalline systems. Crucially, it can be efficiently computed with plane-wave-based DFT methods, since the projector matrix elements are an output of the calculation. Consequently, this method is suitable for high-throughput identification of noncrystalline topological materials. Note that Eq. (2) can also be computed using a localized-basis DFT code, by determining the plane-wave coefficients using a Fourier transform.

Structural spillage in the tight-binding approximation. Defining a structural spillage that is useful in the tight-binding approximation requires us to develop further Eq. (2). The reason is that two issues emerge as we define plane-wave states projected into the tight-binding Hilbert space of N_{sites} as $|\mathbf{p}\alpha\rangle = \frac{1}{\sqrt{N_{\text{sites}}}} \sum_{\mathbf{r}} e^{i\mathbf{p}\cdot\mathbf{r}} |\mathbf{r}\alpha\rangle$, where \mathbf{r} labels the position of each site and α labels internal quantum numbers, such as spin or the orbital type. First, because the tight-binding model's Hilbert space does not span the entire real space but only positions defined by the charge centers, our plane waves are nonorthogonal. Therefore, their overlap depends on the atomic positions, and therefore on the amount of structural disorder. Since we expect continuous translational symmetry to be recovered after averaging over different disorder realizations, we may solve this issue by neglecting the scattering between different momenta in Eq. (2), i.e., assuming that $P_{\mathbf{p},\mathbf{p}'}^{\alpha\beta} \propto \delta_{\mathbf{p},\mathbf{p}'}$. This assumption has been successfully used to determine the topology of noncrystalline systems using the effective Hamiltonian approach [14,20,21,38].

A second issue of the tight-binding approximation is that the projected plane waves form an overcomplete set. A well-defined basis for a crystal with $N_{\text{s/c}}$ sites per unit cell consist of a subset with momenta in $N_{\text{s/c}}$ Brillouin zones. However, there are different types of Brillouin zones depending on the phase factor $e^{i\mathbf{G}\cdot\mathbf{t}}$, where \mathbf{t} are the relative positions of the sites inside the unit cell [65]. For instance, in the honeycomb lattice there are 3 types of BZ, since $e^{-i\mathbf{G}\cdot\mathbf{t}} = e^{ia2\pi/3}$, with $a \in \mathbb{Z}_3$ (see Supplemental Material (SM) [66] C). This issue can be handled by replacing the sum over reciprocal lattice vectors \mathbf{G} by an average over the different types of \mathbf{G} , and multiplying by $N_{\text{s/c}}$.

With these modifications, the structural spillage Eq. (2) can be defined in the tight-binding approximation as

$$\gamma_{\text{qB}}^{\text{TB}}(\mathbf{k}) = \frac{1}{2} \frac{N_{\text{s/c}}}{N_{\text{BZs}}} \sum_{\mathbf{G} \in \text{BZs}} \text{tr}[(P_{\mathbf{k}+\mathbf{G}} - \tilde{P}_{\mathbf{k}+\mathbf{G}})^2], \quad (3)$$

where the sum over \mathbf{G} runs over one BZ of each of the N_{BZs} types, the trace acts over the internal degrees of freedom α ,

and we have defined the single-momentum projector $P_{\mathbf{p}}^{\alpha\beta} = P_{\mathbf{p},\mathbf{p}}^{\alpha\beta}$.

Equations (3) and (2) define the structural spillage to be used in the tight-binding approximation and first-principles calculations, respectively. In the remainder of the paper, we demonstrate how they capture topological phase transitions of amorphous systems, using low-dimensional bismuth as an example.

Tight-binding benchmark: bismuthene on a substrate. Crystalline bismuthene consists of a two-dimensional (2D) honeycomb monolayer of bismuth atoms. Experiments suggest it to be a quantum spin Hall insulator with topological helical edge states when grown on SiC(0001) [81] or Ag(111) [82] substrates. The effect of the substrate is crucial: it filters the p_z orbitals away from the Fermi level leaving the $p_{x,y}$ orbitals, resulting in a large gap ($\sim 0.67\text{eV}$) and a nonzero strong \mathbb{Z}_2 topological index. Moreover, amorphous bismuthene on a substrate is predicted to remain topological via first-principles calculations [13,62], making it a convenient system to benchmark our proposed structural spillage.

The low-energy physics of bismuthene is captured by a tight-binding model with $p_{x,y}$ orbitals in the honeycomb lattice, coupled by nearest-neighbor hoppings t_σ and t_π , a large onsite SOC λ , and a substrate-induced Rashba SOC λ_R (which we take proportional to λ) [81]. To extend this model to amorphous structures while preserving the short-range order expected in amorphous systems [40], we use the voronization of a pointset [8,14] (see SM [66] (A1)). When the pointset is triangular, the voronization produces its dual honeycomb lattice. By randomly displacing the triangular pointset according to a characteristic length r , the voronization produces lattices with threefold coordination, as the honeycomb lattice, but with a finite density of nonhexagonal plaquettes [see Fig. 2(a)] [83]. Therefore, r continuously controls how amorphous are our lattices, allowing us to study the effect of structural disorder on topological properties. In the following, we quantify how amorphous our systems are by the (configuration-averaged) density of nonhexagonal plaquettes $\rho_{\text{non-hex}}$, which is in one-to-one correspondence to the parameter r (see SM [66] (A1)).

In Fig. 2 we present the topological phase diagram of amorphous bismuthene as a function of $\rho_{\text{non-hex}}$ and λ , benchmarking $\gamma_{\text{qB}}^{\text{TB}}(\mathbf{k})$ against the two-terminal conductance results. In the crystalline limit $\rho_{\text{non-hex}} = 0$, the system starts as a Dirac semimetal for vanishing λ , and a finite λ opens up a topological gap, similarly to graphene [84]. Above a critical λ , where the gap closes at the Γ point, the system becomes a topologically trivial insulator, adiabatically connected to the atomic limit in which only the onsite SOC is nonzero.

Both the conductance [Fig. 2(c)] and the structural quasi-Bloch spillage [Fig. 2(d)] capture the topological transition, even at finite structural disorder $\rho_{\text{non-hex}} \neq 0$. The conductance in the topological insulator phase is equal to $2e^2/h$, originating from the helical edge states, while it reduces to zero after the phase transition to the trivial insulator. Concomitantly, $\gamma_{\text{qB}}^{\text{TB}}(\mathbf{k} = 0)$ is large in the topological phase and small in the trivial phase because we choose the reference system to be a trivial crystal, only with nonzero onsite λ . Had we chosen the topological state as reference, the magnitude of the spillage in

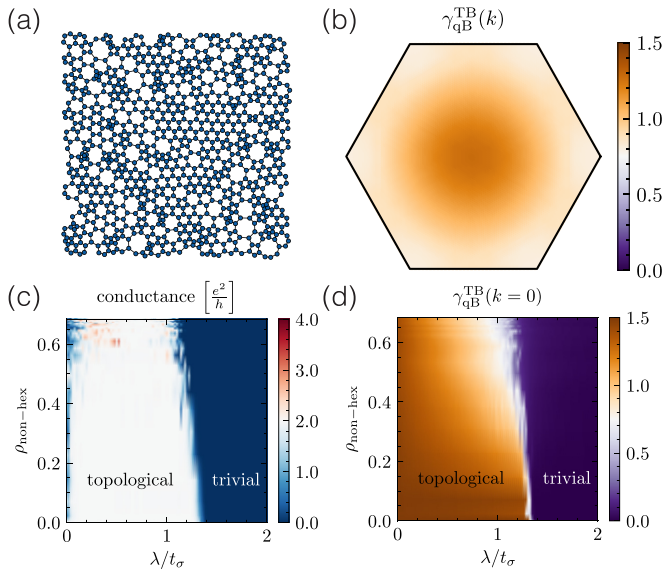


FIG. 2. Structural spillage in the tight-binding approximation. (a) Example of a real-space structure with a density of nonhexagonal plaquettes $\rho_{\text{non-hex}} \simeq 0.53$. (b) Structural quasi-Bloch spillage $\gamma_{\text{qB}}^{\text{TB}}(\mathbf{k})$ in the BZ comparing topological amorphous bismuthene with $\rho_{\text{non-hex}} \simeq 0.53$ and $\lambda = 0.22t_\sigma$ with a trivial crystal with $\lambda/t_\sigma = \infty$. (c), (d) Phase diagrams as a function of SOC λ and the density of nonhexagonal plaquettes $\rho_{\text{non-hex}}$. (c) Conductance in the “armchair” ribbon configuration (see Supplementary Material [66] Eq. (A3)). (d) Structural quasi-Bloch spillage $\gamma_{\text{qB}}^{\text{TB}}(\mathbf{k} = 0)$ comparing the amorphous system to a trivial crystal with $\lambda/t_\sigma = \infty$.

each phase would be inverted, see SM [66] (A1). The critical λ at the transition for the crystal is correctly predicted by $\gamma_{\text{qB}}^{\text{TB}}(\mathbf{k} = 0)$. In agreement with Refs. [13,62], we find that increasing disorder decreases the topological gap and hence the critical λ . Nevertheless, the realistic value of $\lambda \simeq 0.22t_\sigma$ [81] lies in the topological phase also in the amorphous case.

Lastly, Fig. 2(b) shows $\gamma_{\text{qB}}^{\text{TB}}(\mathbf{k})$ for fixed $\lambda = 0.22t_\sigma$ and $\rho_{\text{non-hex}} = 0.53$. $\gamma_{\text{qB}}^{\text{TB}}(\mathbf{k})$ is peaked around $\mathbf{k} = 0$ with a value ~ 1.5 , reminiscent of the crystalline topological band inversion occurring at the Γ point. We also notice that, in the absence of Rashba SOC, the model reduces to two time-reversed copies of Chern insulators. Each copy contributes equally to the structural spillage, demonstrating that the structural spillage works also for other symmetry classes.

Structural spillage in DFT: free-standing Bi bilayer. To show that Eq. (2) is well suited for high-throughput screening of amorphous topological materials, we calculate the structural spillage from the output wavefunctions of first-principles calculations (see full details in SM [66]). We choose previously-studied free-standing bismuth (111) bilayer as an example. This 2D bismuth allotrope, whose crystalline phase consists of a buckled honeycomb lattice with lattice constant $a = 4.33 \text{ \AA}$, is also predicted to be a strong topological insulator crystal with $\mathbb{Z}_2 = 1$ [85–88]. However, no prediction exists for its amorphous counterpart.

To represent amorphous structures given the periodic boundary conditions of the calculations, we create $5 \times 5 \times 1$ supercells comprising of 50 Bi atoms per bilayer. Their electronic structure is calculated for a single supercell momentum,

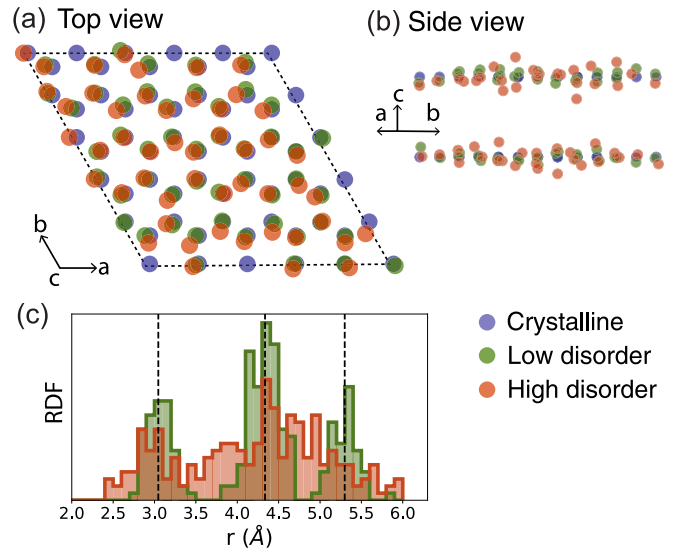


FIG. 3. Bismuth bilayer supercells used in DFT calculations. (a) and (b) show in-plane and out-of-plane views of the supercell, respectively. The colors indicate different degrees of disorder: crystal (blue), low disorder (green) and high disorder (orange). (c) Radial distribution function (RDF) showing the statistics of the bond lengths in the disordered bismuth bilayer and their deviations from the perfect crystal (vertical dashed lines). The disorder is sampled from a Gaussian distribution with a standard deviation of 0.15 \AA for the low disorder and 0.30 \AA for the high disorder.

the center of the supercell BZ. Starting from a crystalline supercell, the structure is disordered by adding random displacements in the x , y , and z directions, sampled from a Gaussian distribution. The structures and their corresponding radial distribution functions are shown in Fig. 3.

To predict the topological phase of amorphous Bi bilayer with SOC, we compute Eq. (2) with plane-wave-based DFT (see SM [66] B) to compare it with its crystalline counterpart without and with SOC. When SOC is not included, and hence when it is topologically trivial (Fig. 4, first row), $\gamma_{\text{qB}}(\mathbf{k})$ is peaked at $\mathbf{k} = 0$, with $\gamma_{\text{qB}}(\mathbf{k} = 0) > 2$. Increasing disorder smooths $\gamma_{\text{qB}}(\mathbf{k})$, yet it remains peaked at Γ with a value greater than 2. In contrast, when we include SOC in calculations of both the disordered Bi bilayer and the pristine crystal (Fig. 4, second row) the spillage is always small. Both rows together show that amorphous bismuth bilayer with SOC is in the same topological state as the crystal with SOC, a strong topological insulator crystal with $\mathbb{Z}_2 = 1$.

We have performed a similar analysis using a tight-binding model for the amorphous Bi (111) bilayer (introduced in SM [66] (A2)). The results, displayed in the last column of Fig. 4, show that for comparable disorder strengths $\gamma_{\text{qB}}^{\text{TB}}(\mathbf{k})$ is broader and its maximum value is smaller than $\gamma_{\text{qB}}(\mathbf{k})$ in DFT. It is thus apparent that, due to the approximations in the tight-binding calculation of the spillage, which lacks information of the real-space extension of the orbitals, the spillage method is more suitable for DFT, an advantageous feature compared to other topological indicators available for noncrystalline systems.

Discussion. We have introduced the structural spillage as an efficient method to signal noncrystalline topological

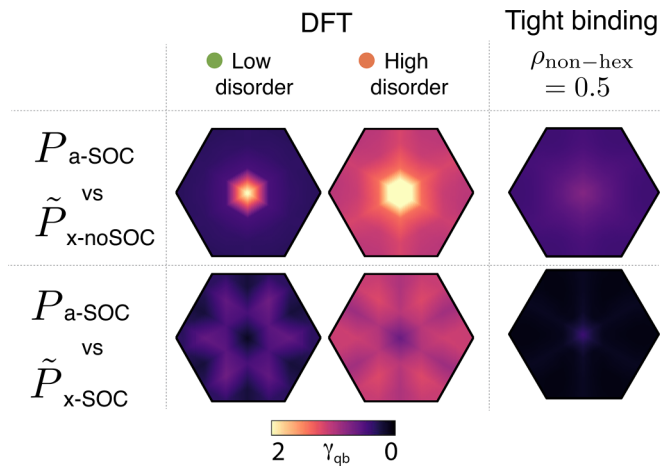


FIG. 4. Structural quasi-Bloch spillage $\gamma_{qb}(\mathbf{k})$ for the bismuth bilayer. First row: comparison between an amorphous system with SOC (a-SOC) and a crystalline system without SOC (x-noSOC). Comparing an amorphous system without SOC with a crystalline sample with SOC leads to similar results. Second row: comparison between the amorphous and crystalline systems with SOC (a-SOC and x-SOC, respectively). $\gamma_{qb}(\mathbf{k})$ is high at $\mathbf{k} = 0$ for the first row while small for the second row, indicating that amorphous bismuth bilayer is a topological insulator. The last column shows a comparison with the tight-binding quasi-Bloch spillage $\gamma_{qb}^{TB}(\mathbf{k})$ (see SM [66] (A2)).

phases, compatible with tight-binding and *ab initio* simulations. We have used it to predict amorphous Bi bilayer as a novel topological insulator.

As was the case for spin-orbit spillage in crystals, we expect the structural spillage to signal a large fraction of promising materials, but not to be infallible: if multiple band inversions are introduced upon amorphization, the spillage might also be artificially large. However, unlike for crystals, the spillage is currently the only systematic, model-independent method that is compatible with *ab initio* calculations. Additionally, we observe that, for different disorder realizations, its fluctuations are smaller compared to scattering methods like calculating the conductance. It can also be applied to systems without a spectral gap, where the effective Hamiltonian approach [38] can fail [14]. Using the spillage in high-throughput calculations implies finding an appropriate crystalline reference. Within noncrystalline structures generated by *ab initio* molecular dynamics, a natural

choice is the seed crystal from which the amorphous phase is obtained. In the few cases where such a reference is absent one may define a plane-wave-resolved spillage (see SM [66] D) by using Eq. (2a) without the sum over \mathbf{G} .

The structural spillage establishes a clear roadmap to construct a high-throughput catalog of noncrystalline (amorphous, polycrystalline, quasicrystalline) topological materials by screening existing amorphous databases, or by scrutinizing realistic structures obtained using existing *ab initio* molecular dynamics packages [89–91]. This methodology may enable for the first time the systematic prediction and discovery of a potentially large number of amorphous materials that are currently inaccessible, suitable to develop affordable and scalable topological devices.

Acknowledgments. We are grateful to S. Franca, F. de Juan, J. Hannukainen, D. López-Cano, R. Queiroz, Q. Marsal, A. Soluyanov, R. M. Martin, J. Vinson, and T. Scaffidi for fruitful discussions and related collaborations. This work was funded by the U.S. Department of Energy, Office of Science, Office of Basic Energy Sciences, Materials Sciences and Engineering Division under Contract No. DE-AC02-05-CH11231 within the Nonequilibrium Magnetic Materials Program (MSMAG), specifically the work by P.C., F.H., and S.M.G., D.M.-S. is supported by an FPU predoctoral contract from Spanish Ministerio de Ciencia, Innovación y Universidades (MCIU) Contract No. FPU19/03195. A.G.G. acknowledges financial support from the European Research Council (ERC) Consolidator grant under Grant Agreement No. 101042707 (TOPOMORPH). D.V. was supported by the Swedish Research Council (VR) and the Knut and Alice Wallenberg Foundation. Computational resources were provided by the National Energy Research Scientific Computing Center and the Molecular Foundry, DOE Office of Science User Facilities supported by the Office of Science, U.S. Department of Energy under Contract No. DEAC02-05CH11231. The work performed at the Molecular Foundry was supported by the Office of Science, Office of Basic Energy Sciences, of the U.S. Department of Energy under the same contract (DEAC02-05CH11231).

The original idea was conceived by P.C. and S.M.G., D.M.-S. derived the expressions for the quasi-Bloch spillage and performed tight-binding calculations assisted by A.G.G., P.C. performed the DFT calculations and developed the spillage code for plane waves assisted by S.M.G., F.H., and D.V. All authors contributed to the interpretation of results and writing of the manuscript. A.G.G. and S.M.G. supervised the project.

- [1] J. Kruthoff, J. de Boer, J. van Wezel, C. L. Kane, and R.-J. Slager, Topological classification of crystalline insulators through band structure combinatorics, *Phys. Rev. X* **7**, 041069 (2017).
- [2] H. C. Po, A. Vishwanath, and H. Watanabe, Symmetry-based indicators of band topology in the 230 space groups, *Nat. Commun.* **8**, 50 (2017).
- [3] Z. Song, T. Zhang, Z. Fang, and C. Fang, Quantitative mappings between symmetry and topology in solids, *Nat. Commun.* **9**, 3530 (2018).

- [4] N. C. Frey, M. K. Horton, J. M. Munro, S. M. Griffin, K. A. Persson, and V. B. Shenoy, High-throughput search for magnetic and topological order in transition metal oxides, *Sci. Adv.* **6**, eabd1076 (2020).
- [5] B. J. Wieder, B. Bradlyn, J. Cano, Z. Wang, M. G. Vergniory, L. Elcoro, A. A. Soluyanov, C. Felser, T. Neupert, N. Regnault, and B. A. Bernevig, Topological materials discovery from crystal symmetry, *Nat. Rev. Mater.* **7**, 196 (2022).
- [6] E. Prodan, Quantum transport in disordered systems under magnetic fields: A study based on operator

- algebras, *Appl. Math. Res. eXpress* **2013**, 176 (2012).
- [7] A. Agarwala and V. B. Shenoy, Topological insulators in amorphous systems, *Phys. Rev. Lett.* **118**, 236402 (2017).
- [8] N. P. Mitchell, L. M. Nash, D. Hexner, A. M. Turner, and W. T. M. Irvine, Amorphous topological insulators constructed from random point sets, *Nat. Phys.* **14**, 380 (2018).
- [9] K. Pöyhönen, I. Sahlberg, A. Westström, and T. Ojanen, Amorphous topological superconductivity in a Shiba glass, *Nat. Commun.* **9**, 2103 (2018).
- [10] C. Bourne and E. Prodan, Non-commutative Chern numbers for generic aperiodic discrete systems, *J. Phys. A: Math. Theor.* **51**, 235202 (2018).
- [11] P. Corbae, S. Ciocys, D. Varjas, E. Kennedy, S. Zeltmann, M. Molina-Ruiz, S. M. Griffin, C. Jozwiak, Z. Chen, L.-W. Wang, A. M. Minor, M. Scott, A. G. Grushin, A. Lanzara, and F. Hellman, Observation of spin-momentum locked surface states in amorphous Bi_2Se_3 , *Nat. Mater.* **22**, 200 (2023).
- [12] Y.-B. Yang, T. Qin, D.-L. Deng, L.-M. Duan, and Y. Xu, Topological amorphous metals, *Phys. Rev. Lett.* **123**, 076401 (2019).
- [13] M. Costa, G. R. Schleder, M. Buongiorno Nardelli, C. Lewenkopf, and A. Fazio, Toward realistic amorphous topological insulators, *Nano Lett.* **19**, 8941 (2019).
- [14] Q. Marsal, D. Varjas, and A. G. Grushin, Topological weaire-thorpe models of amorphous matter, *Proc. Natl. Acad. Sci. USA* **117**, 30260 (2020).
- [15] I. Sahlberg, A. Westström, K. Pöyhönen, and T. Ojanen, Topological phase transitions in glassy quantum matter, *Phys. Rev. Res.* **2**, 013053 (2020).
- [16] A. G. Grushin, Topological phases of amorphous matter, in *Low-Temperature Thermal and Vibrational Properties of Disordered Solids*, edited by M. A. Ramos (World Scientific, Europe, 2022).
- [17] A. Agarwala, V. Juričić, and B. Roy, Higher-order topological insulators in amorphous solids, *Phys. Rev. Res.* **2**, 012067(R) (2020).
- [18] P. Mukati, A. Agarwala, and S. Bhattacharjee, Topological and conventional phases of a three-dimensional electronic glass, *Phys. Rev. B* **101**, 035142 (2020).
- [19] P. Corbae, F. Hellman, and S. M. Griffin, Structural disorder-driven topological phase transition in noncentrosymmetric BiTeI , *Phys. Rev. B* **103**, 214203 (2021).
- [20] H. Spring, A. R. Akhmerov, and D. Varjas, Amorphous topological phases protected by continuous rotation symmetry, *SciPost Phys.* **11**, 022 (2021).
- [21] Q. Marsal, D. Varjas, and A. G. Grushin, Obstructed insulators and flat bands in topological phase-change materials, *Phys. Rev. B* **107**, 045119 (2023).
- [22] J.-H. Wang, Y.-B. Yang, N. Dai, and Y. Xu, Structural-disorder-induced second-order topological insulators in three dimensions, *Phys. Rev. Lett.* **126**, 206404 (2021).
- [23] C. Wang, T. Cheng, Z. Liu, F. Liu, and H. Huang, Structural amorphization-induced topological order, *Phys. Rev. Lett.* **128**, 056401 (2022).
- [24] J. Ma and H. Huang, Amorphous Kane-Mele model in disordered hyperuniform two-dimensional networks, *Phys. Rev. B* **106**, 195150 (2022).
- [25] S. Manna, S. K. Das, and B. Roy, Noncrystalline topological superconductors, [arXiv:2207.02203](https://arxiv.org/abs/2207.02203).
- [26] P. Corbae, J. D. Hannukainen, Q. Marsal, D. Muñoz-Segovia, and A. G. Grushin, Amorphous topological matter: Theory and experiment, *Europhys. Lett.* **142**, 16001 (2023).
- [27] I. Sahlberg, M. N. Ivaki, K. Pöyhönen, and T. Ojanen, Quantum Hall effect and Landau levels without spatial long-range correlations, *Phys. Rev. Res.* **5**, 033218 (2023).
- [28] Y. E. Kraus, Y. Lahini, Z. Ringel, M. Verbin, and O. Zilberberg, Topological states and adiabatic pumping in quasicrystals, *Phys. Rev. Lett.* **109**, 106402 (2012).
- [29] F. Mei, S.-L. Zhu, Z.-M. Zhang, C. H. Oh, and N. Goldman, Simulating \mathbb{Z}_2 topological insulators with cold atoms in a one-dimensional optical lattice, *Phys. Rev. A* **85**, 013638 (2012).
- [30] Y. E. Kraus, Z. Ringel, and O. Zilberberg, Four-dimensional quantum Hall effect in a two-dimensional quasicrystal, *Phys. Rev. Lett.* **111**, 226401 (2013).
- [31] K. A. Madsen, E. J. Bergholtz, and P. W. Brouwer, Topological equivalence of crystal and quasicrystal band structures, *Phys. Rev. B* **88**, 125118 (2013).
- [32] M. Verbin, O. Zilberberg, Y. E. Kraus, Y. Lahini, and Y. Silberberg, Observation of topological phase transitions in photonic quasicrystals, *Phys. Rev. Lett.* **110**, 076403 (2013).
- [33] X. Deng and L. Santos, Topological transitions of interacting bosons in one-dimensional bichromatic optical lattices, *Phys. Rev. A* **89**, 033632 (2014).
- [34] D.-T. Tran, A. Dauphin, N. Goldman, and P. Gaspard, Topological Hofstadter insulators in a two-dimensional quasicrystal, *Phys. Rev. B* **91**, 085125 (2015).
- [35] M. A. Bandres, M. C. Rechtsman, and M. Segev, Topological photonic quasicrystals: Fractal topological spectrum and protected transport, *Phys. Rev. X* **6**, 011016 (2016).
- [36] I. C. Fulga, D. I. Pikulin, and T. A. Loring, Aperiodic weak topological superconductors, *Phys. Rev. Lett.* **116**, 257002 (2016).
- [37] A. Lau, J. van den Brink, and C. Ortix, Topological mirror insulators in one dimension, *Phys. Rev. B* **94**, 165164 (2016).
- [38] D. Varjas, A. Lau, K. Pöyhönen, A. R. Akhmerov, D. I. Pikulin, and I. C. Fulga, Topological phases without crystalline counterparts, *Phys. Rev. Lett.* **123**, 196401 (2019).
- [39] O. Zilberberg, Topology in quasicrystals [Invited], *Opt. Mater. Express* **11**, 1143 (2021).
- [40] R. Zallen, *The Physics of Amorphous Solids* (Wiley-VCH, Weinheim, 1998).
- [41] M. Le Gallo and A. Sebastian, An overview of phase-change memory device physics, *J. Phys. D* **53**, 213002 (2020).
- [42] A. J. Uría-Álvarez, D. Molpeceres-Mingo, and J. J. Palacios, Deep learning for disordered topological insulators through entanglement spectrum, [arXiv:2201.13306](https://arxiv.org/abs/2201.13306).
- [43] A. Kitaev, Anyons in an exactly solved model and beyond, *Ann. Phys. January Special Issue*, **321**, 2 (2006).
- [44] E. Prodan, Non-commutative tools for topological insulators, *New J. Phys.* **12**, 065003 (2010).
- [45] R. Bianco and R. Resta, Mapping topological order in coordinate space, *Phys. Rev. B* **84**, 241106(R) (2011).
- [46] A. Marrazzo and R. Resta, Locality of the anomalous Hall conductivity, *Phys. Rev. B* **95**, 121114(R) (2017).
- [47] Z. Li and R. S. K. Mong, Local formula for the \mathbb{Z}_2 invariant of topological insulators, *Phys. Rev. B* **100**, 205101 (2019).
- [48] T. A. Loring and H. Schulz-Baldes, The spectral localizer for even index pairings, *J. Noncommutative Geom.* **14**, 1 (2020).

- [49] H. Schulz-Baldes and T. Stoiber, The spectral localizer for semifinite spectral triples, *Proc. Am. Math. Soc.* **149**, 121 (2021).
- [50] M. Guzmán, D. Bartolo, and D. Carpentier, Geometry and topology tango in ordered and amorphous chiral matter, *SciPost Phys.* **12**, 038 (2022).
- [51] A. Cerjan and T. A. Loring, Local invariants identify topology in metals and gapless systems, *Phys. Rev. B* **106**, 064109 (2022).
- [52] P. d'Ornellas, R. Barnett, and D. K. K. Lee, Quantized bulk conductivity as a local Chern marker, *Phys. Rev. B* **106**, 155124 (2022).
- [53] A. Cerjan and T. A. Loring, An operator-based approach to topological photonics, *Nanophotonics* **11**, 4765 (2022).
- [54] J. D. Hannukainen, M. F. Martínez, J. H. Bardarson, and T. K. Kvarning, Local topological markers in odd spatial dimensions and their application to amorphous topological matter, *Phys. Rev. Lett.* **129**, 277601 (2022).
- [55] W. Chen, Universal topological marker, *Phys. Rev. B* **107**, 045111 (2023).
- [56] D. Ceresoli and R. Resta, Orbital magnetization and Chern number in a supercell framework: Single \mathbf{k} -point formula, *Phys. Rev. B* **76**, 012405 (2007).
- [57] R. Favata and A. Marrazzo, Single-point spin Chern number in a supercell framework, *Electron. Struct.* **5**, 014005 (2023).
- [58] S. M. Griffin and N. A. Spaldin, On the relationship between topological and geometric defects, *J. Phys.: Condens. Matter* **29**, 343001 (2017).
- [59] J. Liu and D. Vanderbilt, Spin-orbit spillage as a measure of band inversion in insulators, *Phys. Rev. B* **90**, 125133 (2014).
- [60] Y.-Z. You, Z. Bi, A. Rasmussen, K. Slagle, and C. Xu, Wave function and strange correlator of short-range entangled states, *Phys. Rev. Lett.* **112**, 247202 (2014).
- [61] J. Y. Lee, Y.-Z. You, and C. Xu, Symmetry protected topological phases under decoherence, [arXiv:2210.16323](https://arxiv.org/abs/2210.16323).
- [62] B. Focassio, G. R. Schleder, M. Costa, A. Fazzio, and C. Lewenkopf, Structural and electronic properties of realistic two-dimensional amorphous topological insulators, *2D Mater.* **8**, 025032 (2021).
- [63] K. Choudhary, K. F. Garrity, and F. Tavazza, High-throughput discovery of topologically non-trivial materials using spin-orbit spillage, *Sci. Rep.* **9**, 8534 (2019).
- [64] K. Choudhary, K. F. Garrity, N. J. Ghimire, N. Anand, and F. Tavazza, High-throughput search for magnetic topological materials using spin-orbit spillage, machine learning, and experiments, *Phys. Rev. B* **103**, 155131 (2021).
- [65] W. S. Jung, C. S. Leem, C. Kim, S. R. Park, S. Y. Park, B. J. Kim, E. Rotenberg, and C. Kim, Imaging the electron density in solids by using multi-Brillouin-zone angle resolved photoelectron spectroscopy, *Phys. Rev. B* **82**, 235105 (2010).
- [66] See Supplemental Material at <http://link.aps.org/supplemental/10.1103/PhysRevResearch.5.L042011> for a discussion of the approximations entering Eq. (3), definition of the tight-binding models, and further benchmarks on their phase diagrams as well as details regarding our DFT calculations, which includes Refs. [67–80].
- [67] W. A. Harrison, *Electronic Structure and the Properties of Solids: The Physics of the Chemical Bond* (Dover Publications, New York, 1989).
- [68] E. H. Lieb, Two theorems on the Hubbard model, *Phys. Rev. Lett.* **62**, 1201 (1989).
- [69] Q. Li, J. S. Smith, Y. Yin, C. Wang, M. V. Klymenko, J. H. Cole, and N. V. Medhekar, Localized Wannier function based tight-binding models for two-dimensional allotropes of bismuth, *New J. Phys.* **23**, 063042 (2021).
- [70] S. Singh, Z. Zanolli, M. Amsler, B. Belhadji, J. O. Sofo, M. J. Verstraete, and A. H. Romero, Low-energy phases of Bi monolayer predicted by structure search in two dimensions, *J. Phys. Chem. Lett.* **10**, 7324 (2019).
- [71] P. Ares, J. J. Palacios, G. Abellán, J. Gómez-Herrero, and F. Zamora, Recent progress on antimonene: A new bidimensional material, *Adv. Mater.* **30**, 1703771 (2018).
- [72] C. W. Groth, M. Wimmer, A. R. Akhmerov, and X. Waintal, Kwant: a software package for quantum transport, *New J. Phys.* **16**, 063065 (2014).
- [73] A. Weiße, G. Wellein, A. Alvermann, and H. Fehske, The kernel polynomial method, *Rev. Mod. Phys.* **78**, 275 (2006).
- [74] D. Varjas, M. Fruchart, A. R. Akhmerov, and P. M. Perez-Piskunow, Computation of topological phase diagram of disordered $\text{Pb}_{1-x}\text{Sn}_x\text{Te}$ using the kernel polynomial method, *Phys. Rev. Res.* **2**, 013229 (2020).
- [75] G. Kresse and J. Furthmüller, Efficient iterative schemes for *ab initio* total-energy calculations using a plane-wave basis set, *Phys. Rev. B* **54**, 11169 (1996).
- [76] G. Kresse and J. Hafner, *Ab initio* molecular dynamics for liquid metals, *Phys. Rev. B* **48**, 13115 (1993).
- [77] J. P. Perdew, K. Burke, and M. Ernzerhof, Generalized gradient approximation made simple, *Phys. Rev. Lett.* **77**, 3865 (1996).
- [78] G. Kresse and D. Joubert, From ultrasoft pseudopotentials to the projector augmented-wave method, *Phys. Rev. B* **59**, 1758 (1999).
- [79] S. P. Ong, W. D. Richards, A. Jain, G. Hautier, M. Kocher, S. Cholia, D. Gunter, V. L. Chevrier, K. A. Persson, and G. Ceder, Python materials genomics (pymatgen): A robust, open-source python library for materials analysis, *Comput. Mater. Sci.* **68**, 314 (2013).
- [80] M. Soriano and J. J. Palacios, Theory of projections with nonorthogonal basis sets: Partitioning techniques and effective Hamiltonians, *Phys. Rev. B* **90**, 075128 (2014).
- [81] F. Reis, G. Li, L. Dudy, M. Bauernfeind, S. Glass, W. Hanke, R. Thomale, J. Schäfer, and R. Claessen, Bismuthene on a SiC substrate: A candidate for a high-temperature quantum spin Hall material, *Science* **357**, 287 (2017).
- [82] S. Sun, J.-Y. You, S. Duan, J. Gou, Y. Z. Luo, W. Lin, X. Lian, T. Jin, J. Liu, Y. Huang, Y. Wang, A. T. S. Wee, Y. P. Feng, L. Shen, J. L. Zhang, J. Chen, and W. Chen, Epitaxial growth of ultraflat bismuthene with large topological band inversion enabled by substrate-orbital-filtering effect, *ACS Nano* **16**, 1436 (2022).
- [83] A. G. Grushin and C. Repellin, Amorphous and polycrystalline routes toward a chiral spin liquid, *Phys. Rev. Lett.* **130**, 186702 (2023).
- [84] C. L. Kane and E. J. Mele, \mathbb{Z}_2 topological order and the quantum spin Hall effect, *Phys. Rev. Lett.* **95**, 146802 (2005).
- [85] S. Murakami, Quantum spin Hall effect and enhanced magnetic response by spin-orbit coupling, *Phys. Rev. Lett.* **97**, 236805 (2006).
- [86] M. Wada, S. Murakami, F. Freimuth, and G. Bihlmayer, Localized edge states in two-dimensional topological insulators: Ultrathin Bi films, *Phys. Rev. B* **83**, 121310(R) (2011).

- [87] Z. Liu, C.-X. Liu, Y.-S. Wu, W.-H. Duan, F. Liu, and J. Wu, Stable nontrivial \mathbb{Z}_2 topology in ultrathin Bi (111) films: A first-principles study, *Phys. Rev. Lett.* **107**, 136805 (2011).
- [88] Z.-Q. Huang, F.-C. Chuang, C.-H. Hsu, Y.-T. Liu, H.-R. Chang, H. Lin, and A. Bansil, Nontrivial topological electronic structures in a single Bi(111) bilayer on different substrates: A first-principles study, *Phys. Rev. B* **88**, 165301 (2013).
- [89] T. D. Kühne *et al.*, Cp2k: An electronic structure and molecular dynamics software package - Quickstep: Efficient and accurate electronic structure calculations, *J. Chem. Phys.* **152**, 194103 (2020).
- [90] B. Focassio, G. R. Schleder, F. Crasto de Lima, C. Lewenkopf, and A. Fazzio, Amorphous Bi₂Se₃ structural, electronic, and topological nature from first principles, *Phys. Rev. B* **104**, 214206 (2021).
- [91] T. F. Harrelson, E. Sheridan, E. Kennedy, J. Vinson, A. T. N'Diaye, M. V. P. Altoé, A. Schwartzberg, I. Siddiqi, D. F. Ogletree, M. C. Scott *et al.*, Elucidating the local atomic and electronic structure of amorphous oxidized superconducting niobium films, *Appl. Phys. Lett.* **119**, 244004 (2021).

Correction: The footnote indicating equal contribution for the first two authors was missing at publication and has been inserted.